Journal of Diabetes Science and Technology
Volume 1, Issue 4, July 2007

SYMPOSIUM

Selectivity Assessment of Noninvasive Glucose Measurements Based on Analysis of Multivariate Calibration Vectors

Mark A. Arnold, Ph.D., Lingzhi Liu, Ph.D., and Jonathon T. Olesberg, Ph.D.

Abstract

Background:
Selectivity is paramount for the successful implementation of noninvasive spectroscopic sensing for the painless measurement of blood glucose concentrations in people with diabetes. Selectivity issues are explored for different multivariate calibration models based on noninvasive near-infrared spectra collected from an animal model.

Methods:
Noninvasive near-infrared spectra are collected through a fiber-optic interface attached to a thin fold of skin on the back of an anesthetized laboratory rat while glucose levels are varied in a controlled manner.

Results and Discussion:
Partial least-squares (PLS) calibration models are generated from noninvasive spectra collected during a single, 2-hour blood glucose transient. Calibration vectors are compared for optimized PLS calibration models created with correct and incorrect assignments of glucose concentrations to each noninvasive spectrum. Although both PLS models appear functional and seem capable of predicting glucose concentrations accurately during this transient, only the model generated from correct glucose assignments gives a credible calibration vector. When correct glucose assignments are used, the PLS calibration vector matches the corresponding net analyte signal calibration vector. No similarity in these calibration vectors is evident when incorrect glucose assignments are used.

Conclusions:
Glucose-specific spectral information is present within noninvasive near-infrared spectra collected from a rat model using a transmission geometry. Apparently functional, yet incorrect, calibration models can be generated, and the propensity to create such false PLS calibration models calls into question the validity of past reports. An analysis of calibration vectors can provide valuable insight into the chemical basis of selectivity for multivariate calibration models of complex systems.

J Diabetes Sci Technol 2007;1(4):454-462

Author Affiliation: Department of Chemistry and Optical Science and Technology Center, University of Iowa, Iowa City, Iowa

Abbreviations: (AU) absorbance units; (DCCT) Diabetes Control and Complications Trial ; (NAS) net analyte signal; (PLS) partial least squares; (RMS) root mean square; (SECV) standard error of cross validation; (SEP) standard error of prediction

Keywords: calibration vector analysis, Clarke error grid analysis, multivariate statistics, near-infrared spectroscopy, net analyte signal, noninvasive glucose sensing

Corresponding Author: Mark A. Arnold, Ph.D., Department of Chemistry and Optical Science and Technology Center, University of Iowa, Iowa City, IA 52242; email address *mark-arnold@uiowa.edu*

Introduction

Tight glycemic control is well recognized as the primary goal in the management of both type 1 and type 2 diabetes. Success demands frequent insulin administration in response to accurate measurement of blood glucose concentrations. Since completion of the Diabetes Control and Complications Trial (DCCT) study in 1993,[1] considerable research efforts have been devoted to the development of novel insulin formulations and convenient blood glucose sensing technology that is compatible with frequent daily monitoring. The result is an impressive array of commercially available home glucose meters that provide sufficiently accurate blood glucose readings for daily monitoring and tight glycemic control. These complex analytical systems report accuracies on the order of 10–15% with blood samples as small as 3 μl in as little as 15 seconds. Still, conventional test-strip glucose meters are limited to single point measurements and require the collection of individual blood samples for each measurement.

Also since the DCCT study, extensive research has focused on the development of continuous, or nearly continuous, blood glucose monitors that can provide valuable information related to changes in glucose concentration. Both the rate and the direction of changes in glucose concen-tration are important pieces of diagnostic information. Most attention in this regard has been given to implantable biosensors that reside for short periods within the subcutaneous tissue. Measurement accuracy limits the utility of these implants, where sensor calibration is adversely affected by the biologic response to the implant.[2,3] Poor biocompatibility limits operation of these implants to 3 days, and glucose readings during the course of operation are not approved for insulin administration, but are valuable for following trends and assessing insulin treatment regimens. The GlucoWatch biographer is an alternative technology capable of providing three glucose readings per hour with each sensing pad capable of continuous operation for 12 hours.[4,5] In this technology, an externally applied current pulls interstitial fluid across the skin and into a sensing pad where the glucose is measured coulometrically and external to the body. Issues of user discomfort and inaccuracies at low glucose concentrations limit the wide spread use of this technology.

Noninvasive glucose sensing is yet another measurement strategy that promises pain-free operation without the complications of an adverse biologic response.[6–8] In the most common implementation, a noninvasive measurement involves the passage of a selected band of electromagnetic radiation through a vascular region of the body. As this light propagates through the tissue, it interacts with the components of the tissue, including glucose. The spectrum of the light exiting the body is collected and analyzed to ascertain the concentration of glucose within the sampled tissue volume. This approach is noninvasive in the sense that nothing is extracted from the body and there is no need to place a physical component inside the body, thereby eliminating problems associated with biocompatibility. Noninvasive measurements offer the promise of being painless, reagentless, fast, convenient, continuous, and biocompatible. In addition, information from multiple analytes is possible depending on the wavelengths used in the analysis.

Selectivity is the most important aspect of noninvasive glucose sensing. For conventional analytical measurements, selectivity is achieved using a combination of physical separations and specific chemical reactions. For glucose sensing, membranes are commonly used to restrict interferences from the measurement location and enzymes are used to convert glucose to a readable form. For noninvasive measurements, physical separations and selective chemical reactions are not possible because there is no direct access to the sample. All the selective analytical information must originate from an analysis of the collected *in vivo* spectra.

This article explores the issue of selectivity for noninvasive glucose measurements from near-infrared spectra collected from an animal model. A series of transmission spectra is collected by passing near-infrared light through a thin fold of skin located on the upper shoulder region of an anesthetized laboratory rat.[9] Spectra are collected continuously as the glucose level is varied in a controlled manner. The resulting *in vivo* spectra are analyzed with a focus on documenting measurement selectively. Emphasis is placed on understanding the chemical basis of the spectroscopic selectivity and demonstrating that this information originates from glucose molecules within the tissue matrix. The propensity to generate nonselective calibration models is also illustrated and discussed.

Methods

Experimental details for the noninvasive spectra used in this work are published elsewhere.[9] A brief summary of these experimental details is provided next.

Apparatus and Instrumentation

Noninvasive spectra were collected with a Thermo-Nicolet Model 670 Fourier transform spectrometer equipped with an external 50-watt tungsten halogen lamp, calcium fluoride beam splitter, and a thermoelectrically cooled extended wavelength indium gallium arsenide detector. Optical filters in the optical path limited the spectral range between 4000 and 5000 cm^{-1}. Light exiting the interferometer is focused into an optical fiber composed of fused silica and this fiber carries the incident light to the skin fold where the spectrum is collected. A C-shaped clamp aligns the incident and detection optical fibers across the fold of skin. Light exiting the skin is collected by the opposing optical fiber, which guides the transmitted light to the detector.

Procedures

Measurements were made with an anesthetized adult male Sprague–Dawley rat. This animal was initially anesthetized with ketamine and anesthesia was maintained with chloralose. Fluids of blank saline or glucose were delivered through a catheter placed in the femoral vein and blood samples were collected periodically from a second catheter placed in the femoral artery. The animal was monitored continuously during anesthesia with a pulse oximeter and rectal thermometer, which provided information about oxygenation, pulse rate, and core body temperature. Body temperatures were maintained at 38°C with a heating pad coupled to a feedback temperature controller.

Figure 1 shows the experimental setup, including the interface showing the optical fibers on an adjustable mount. This interface was positioned on a shaved fold of skin located on the upper shoulder region of the rat. Near-infrared spectra collected from this region are similar in shape to noninvasive spectra collected from skin on the back of the hand of human subjects. A principal feature of such noninvasive spectra is the absence of absorption bands related to fat cells.

Noninvasive spectra were collected continuously during the experiment, which generated 360 single beam spectra over a period of 7 hours. Each spectrum was collected as 128 co-added interferograms with resolution of 16 cm^{-1}. Each spectrum required a little more than 60 seconds for collection. The root mean square (RMS) noise was 15 microabsorbance units (μAU) as measured from 100% lines generated from a tissue phantom composed of 1 mm water combined with a 1.8-AU neutral density filter. These RMS noise levels were computed from a second-order polynomial fit of these 100% lines over a spectral range from 4400 to 4500 cm^{-1}.[6] A tissue phantom composed of water and a neutral density filter does not include features associated with protein and other molecular components of the skin tissue. Nevertheless, this simple tissue phantom provides radiant powers at the detector that match those generally observed for samples of human and rat skin, which is perfect to assess the instrumental signal-to-noise ratio of the measurement.

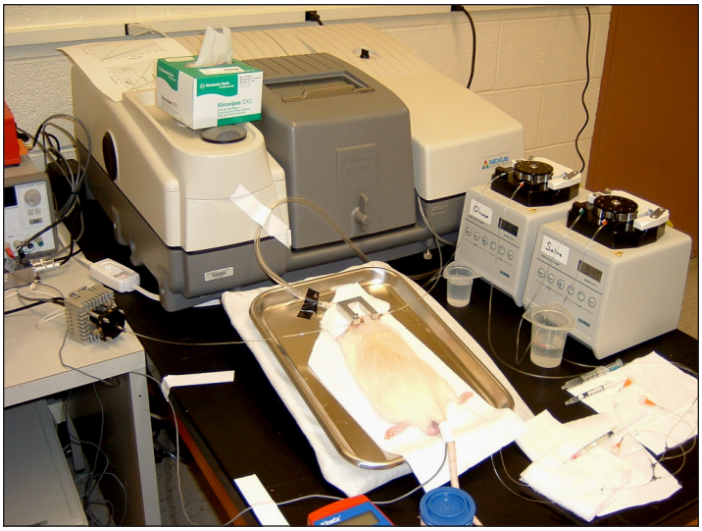

Figure 1. Noninvasive data collection experiment showing the anesthetized animal coupled to the Fourier transform spectrometer through a fiber-optic interface connected to a fold of skin on the back of the animal.

A single glucose transient was generated while collecting noninvasive spectra. Initially, glucose levels were maintained nearly constant with values ranging between 5 and 10 m*M*. After 3 hours, the glucose level was increased steeply by infusing a solution composed of 50% glucose dissolved in saline. This glucose solution was infused continuously for 2 hours at a rate of 2 ml/h. The arterial blood glucose concentration peaked at approximately 33 m*M* or 600 mg/dl. Blood glucose concentrations were monitored throughout by collecting arterial blood samples periodically. These samples were analyzed with a HemoCue Glucose 201 analyzer.

Results and Discussion

Many reported noninvasive glucose experiments follow a procedure where spectra are collected periodically during an oral glucose tolerance test. The corresponding glucose transient is quantified using reference glucose concentrations measured in a series of blood samples. Glucose concentrations are assigned to each spectrum through interpolation. Generally, a time lag is added to account for dynamics between the concentration of

glucose in blood and interstitial fluid. This lag time is a consequence of the fact that the noninvasive spectrum is obtained primarily through interstitial fluid rather than blood, and some time is required for glucose transport from the blood to the tissue. In many cases, different lag times are tried until the best results are obtained.

The resulting noninvasive spectra are combined with the assigned glucose concentrations to prepare a calibration model that predicts *in vivo* glucose concentrations. Procedurally, the full set of spectral data is randomly divided into two groups, where one group is used to generate the calibration model and the second group is used to validate model accuracy. This first group is called calibration data and is used to establish a calibration vector that represents the best correlation between spectral variance and glucose concentration predictions. The predicted concentration of glucose is obtained as the inner product between the sample spectrum and this calibration vector. The primary objective is to generate a calibration vector that provides accurate and robust predictions of glucose concentration from noninvasive spectra collected subsequently to the calibration data.

Statistical methods, such as partial least-squares (PLS) regression or artificial neural networks, are typically used to generate the calibration vector for a targeted analyte. In these methods, variations within spectral data are statistically correlated to changes in glucose concentration. The working assumption is that the spectral variations that correlate most strongly with changes in concentration can be used to predict glucose concentrations in spectra generated from subsequent samples. It is important to understand, however, that there is no conditional requirement that the principal spectral variance originates from the molecular structure of glucose. Indeed, these algorithms do not require molecule specificity, only statistical significance in the correlations. By design, these algorithms can discern tiny correlations within these data sets, even if the correlation originates from ambiguous sources, such as noise or spectral drift.

The efficiency of the PLS algorithm to establish correlations between spectral variance and analyte concentration makes this a popular method for generating calibration vectors for noninvasive measurements. Unfortunately, the blind acceptance of results of this algorithm can result in calibration models that are based on drifts, noise, and spurious correlations. Powerful insight can be gained by understanding the origin of the information embedded within the calibration vector.

PLS Calibration Model from Noninvasive Rat Spectra

A calibration model based on the PLS algorithm was developed from noninvasive spectra collected from the animal model. In this analysis, 360 noninvasive spectra were randomly split with 306 spectra (85%) used as calibration data and the remaining 54 spectra (15%) used for model validation (prediction data). The PLS calibration vector was determined over a spectral range of 4900–4200 cm^{-1} with nine PLS factors. This number of factors was deemed optimal by comparing the standard error of cross validation (SECV) as a function of number of factors for 50 repeated leave one-third-out cross validation calculations.[8] SECV was calculated according to the following equation for each repeat of the one-third left-out splitting of calibration data and for each number of factors:

$$\mathrm{SECV} = \sqrt{\frac{\sum (x_i - \hat{x}_i)^2}{n_{CV}}}$$

where x_i is the assigned glucose concentration for spectrum i in the one-third left-out spectra, $\hat{x}_i$ is the corresponding concentration of glucose predicted from the calibration model for spectrum i, and n_{CV} is the number of spectra in the one-third left-out cross validation, which is 102 spectra in this case. A lower SECV indicates greater model accuracy as the difference between assigned and model-predicted glucose concentrations is smaller.

Figure 2 shows the impact of number of factors on model performance. As is typical of PLS calibration models, the standard error decreases to a minimum as more factors are used in the analysis. For these data, the minimum is reached at 12 factors. An *F*-test statistical analysis is used to determine the fewest number of factors for which the SECV is not significantly different than the minimum at the 90% confidence level. For these data, the optimum number of factors is nine. The calibration data set has a sufficient number of independent spectra to support this number of factors. In general, six independent spectra are needed to justify each factor in the calibration on the basis of degrees of freedom.[10] In this experiment, calibration data consist of 204 spectra (306 – 102) and, therefore, can accommodate a maximum of 34 factors.

The final parameter to be established for the calibration model is the lag time between arterial blood glucose measurements and assigned tissue levels of glucose for each spectrum. In this work, a 15-minute lag time was applied to the arterial glucose readings, which is consistent with values measured with implantable biosensors.[11]

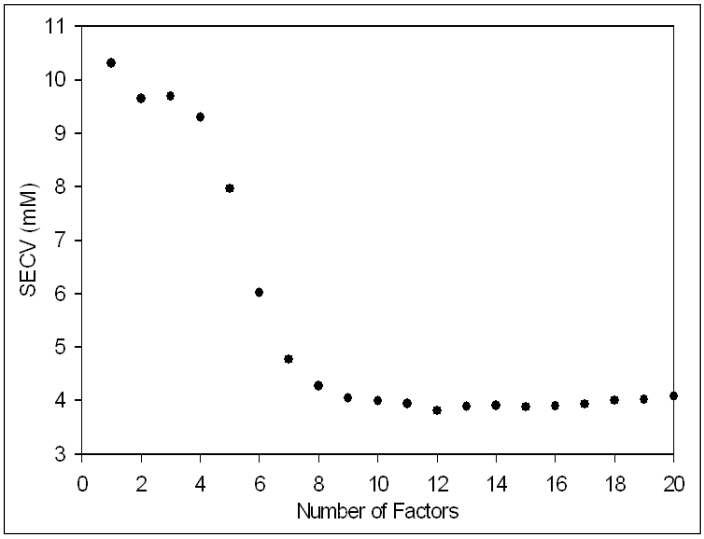

Figure 2. Effect of number of factors used in the PLS calibration model on model performance, showing minimum standard errors with 12 factors.

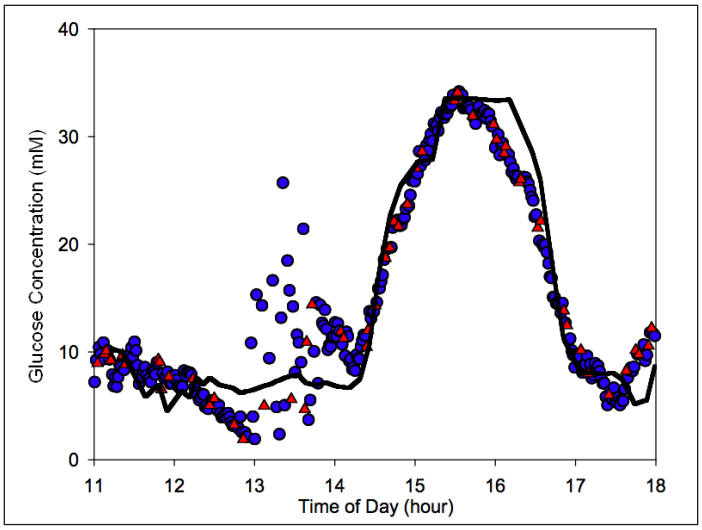

Figure 3. Glucose–time plot for PLS calibration model showing calibration points (blue circles), prediction points (red triangles), and arterial blood glucose concentrations with a 15-minute lag time (black line).

Results of the PLS calibration model are presented in **Figure 3** in the form of a glucose–time profile. In this plot, the predicted concentrations of glucose are plotted as a function of time where circles represent glucose concentrations predicted from spectra used in calibration data and triangles represent concentrations obtained from prediction spectra. The solid black line represents the estimated tissue glucose levels, which correspond to the measured blood glucose concentrations shifted 15 minutes to the right. The standard error of prediction (SEP) for prediction data points is 1.98 m*M* across all predictions, where SEP is calculated according to the following equation:

$$\mathrm{SEP} = \sqrt{\frac{\sum (x_i - \hat{x}_i)^2}{n_P}}$$

where x_i is the assigned glucose concentration for spectrum i in the prediction data set, $\hat{x}_i$ is the corresponding concentration of glucose predicted from the calibration model for spectrum i, and n_p is the number of spectra in the prediction data set (54 in this experiment).

A noteworthy aspect of the time profile in **Figure 3** is the large scattering of points just before the glucose transient. This scattering of points corresponds to the period between 1300 and 1345 hours when the fiber-optic interface was purposely removed and resecured before collecting each spectrum. Resetting the interface before each spectrum creates a significant amount of variance, which is likely caused by slight differences in various components of the tissue matrix within the optical region. Changes in the amount of water, protein, fat, and scattering properties of skin are evident in spectra collected during this period as characterized elsewhere.[9] The large variations associated with resetting the fiber-optic interface contributes to the large SEP (1.98 m*M*) noted earlier for this calibration model.

PLS Calibration Model with Incorrect Glucose Concentration Assignments

An interesting exercise is to repeat the PLS analysis of noninvasive spectral data after purposely assigning incorrect glucose concentrations to each spectrum. Incorrect glucose concentrations should result in poor models and an inability to predict glucose concentrations accurately. Two different types of incorrect glucose assignments are used to illustrate the effectiveness of this approach.

First, glucose concentrations are assigned randomly to spectra over a concentration range of 5 to 35 m*M* and the PLS calibration model is regenerated by the same procedures described earlier. Results are presented in **Figure 4** for the resulting PLS model. These results are presented as a concentration correlation plot where the concentration of glucose predicted from the PLS model is plotted as a function of the randomly assigned glucose concentration. No systematic correlation is apparent in this plot and the SEP is 13.3 m*M*, which is essentially the same as the standard deviation of the randomly assigned glucose concentrations. These results indicate that this PLS model has no ability to predict glucose, as expected for incorrect glucose assignments.

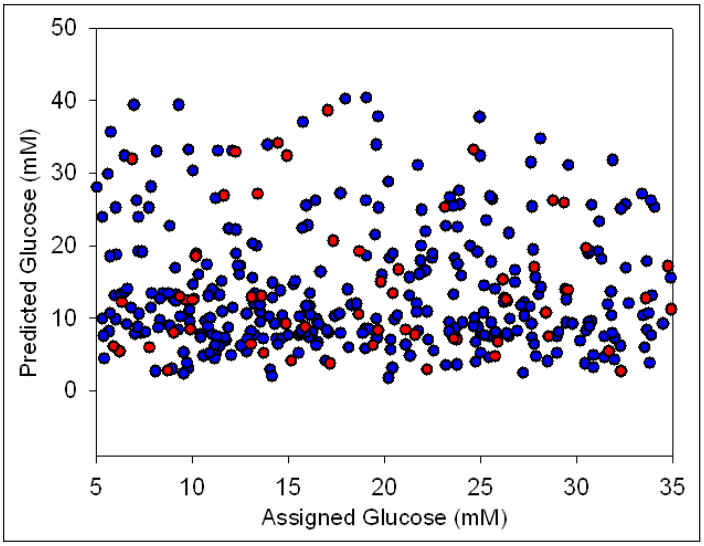

Figure 4. Concentration correlation plot for a PLS calibration model generated from noninvasive spectra with randomly assigned incorrect glucose concentrations showing calibration points (blue) and prediction points (red).

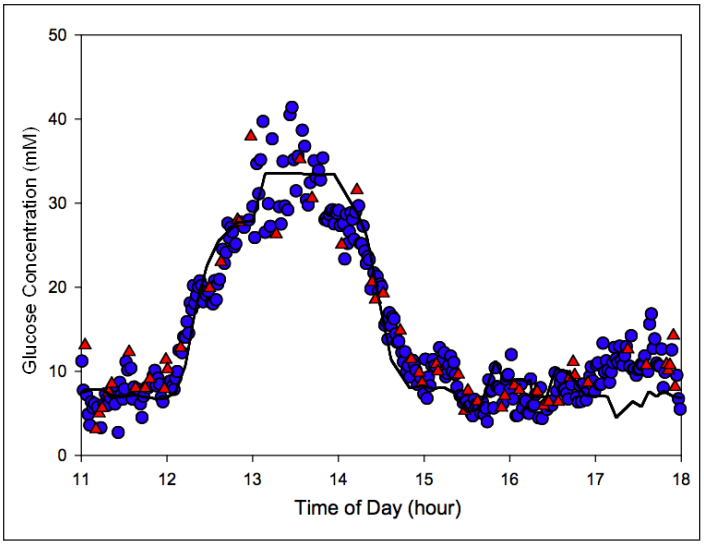

Figure 5. Glucose–time plot for a PLS calibration model generated from nonrandom but incorrectly assigned glucose concentrations showing calibration points (blue circles), prediction points (red triangles), and arterial blood glucose concentrations incorrectly shifted forward by 2 hours (black line).

The second type of incorrect glucose assignment studied here is to shift the glucose transient forward by 2 hours. Instead of the initial transient starting at 1400 hours, glucose concentrations are assigned as if the transient had started at 1200 hours. Basically, the entire time profile is shifted forward by 2 hours and reference concentration values obtained before 1300 are wrapped around to the end of the transient. In this experiment, the blood glucose concentration actually measured for the arterial blood sample collected at 1300 hours is assigned incorrectly to the noninvasive spectrum collected at 1100 hours.

Results from the corresponding PLS calibration model are presented in **Figure 5**. This incorrect PLS model uses 13 factors and appears to provide excellent predictions of glucose concentrations for both calibration and prediction data points. The computed SEP is only 3.2 m*M*. Furthermore, a Clarke error grid analysis[12] of these model predictions (plot not shown) reveals that 99% of the model results (calibration and prediction data combined) fall within the acceptable A–B regions, whereas only 1% of these predictions falls in the C region and none of the observations falls in the D or E regions.

Results from the Clarke error grid analysis and the ability to closely track the glucose transient rival or surpass published accounts of alleged noninvasive glucose measurements. The problem is, of course, the values reported by this model are invalid. Because the glucose assignments are incorrect, the resulting calibration model cannot possibly be predicting glucose concentrations on the basis of glucose-specific information.

It is noteworthy that random glucose assignments did not produce an apparently functional calibration. The time dependency of this second type of incorrect assignment produces temporal correlations within spectral data that correlate to the time-dependent variations of the glucose concentrations, thereby providing a basis for the PLS regression model and an apparently functional calibration.

Most importantly, the false calibration model represented in **Figure 5** calls into question the validity of the calibration model with the correct glucose assignments (**Figure 3**). Without further analysis, it is impossible to conclude that glucose is being measured in **Figure 3** owing to the known incorrectness of the model represented in **Figure 5**. Most literature reports that claim successful noninvasive glucose measurements are subject to this criticism because no additional proof is provided to corroborate findings from the PLS model alone.

Analysis of Calibration Vectors

The calibration vector is the final product of the PLS algorithm and represents the component of sample spectra that best predicts analyte concentrations. The inner product of the calibration vector and a sample spectrum produces a scalar quantity that represents the predicted concentration of the targeted analyte in the sample. Both the shape and the magnitude of the calibration vector are important for measurement accuracy. The shape defines measurement selectivity and the magnitude defines measurement sensitivity.

A calibration vector can be thought of as a filter that passes information related to the analyte while suppressing signals originating from interferences. In the simplest case where the analyte and interferences have nonoverlapping signals, the shape of the calibration vector will match the spectrum of the analyte. In near-infrared spectroscopy, however, the analyte signal generally overlaps with signals from the matrix components and the resulting shape of the calibration vector is considerably more complex. The filtering properties of a calibration vector with over-lapping spectra must maximize the amount of analyte information that passes while minimizing the passage of interfering signals. The impact of an overlapping and interfering signal can only be minimized by dividing the interfering signal in half, integrating each half separately, and then subtracting these two areas. Using this strategy, the final integrated signal from an interfering signal sums to zero regardless of the concentration of the interfering substance. In practice, this process to remove overlapping signals is accomplished with a combination of positive and negative components to the calibration vector.

Examples of calibration vectors are presented in **Figure 6** where **Figure 6A** shows the calibration vector for the PLS calibration model based on correct glucose assignments and **Figure 6B** presents the calibration vector for the model based on the nonrandom incorrect glucose assignments described earlier. Both have positive and negative features, which are necessary to pass analyte information and suppress interfering signals. A more detailed interpretation of the shape of these calibration vectors is nearly impossible owing to the chemical complexity of the sample matrix and the degree of spectral overlap between matrix components. Nevertheless, the difference in the shapes of these two calibration vectors is highly significant.

Superimposed on each PLS calibration vector in **Figure 6** is the calibration vector generated by the net analyte signal (NAS) computed for glucose in this rat skin tissue matrix.[9] The term NAS was first introduced by Lober to describe that component of the analyte spectrum that is orthogonal to all interfering sources of spectra variance within the data set.[13,14] The NAS, therefore, represents the selective component of the analyte spectrum relative to the spectral background generated by the spectral variance created by changes in the sample matrix, instrumentation, and environment.

The concept of the NAS calibration vector presented in **Figure 6** and the procedures for its creation are described in detail elsewhere.[9] Briefly, the NAS is determined from

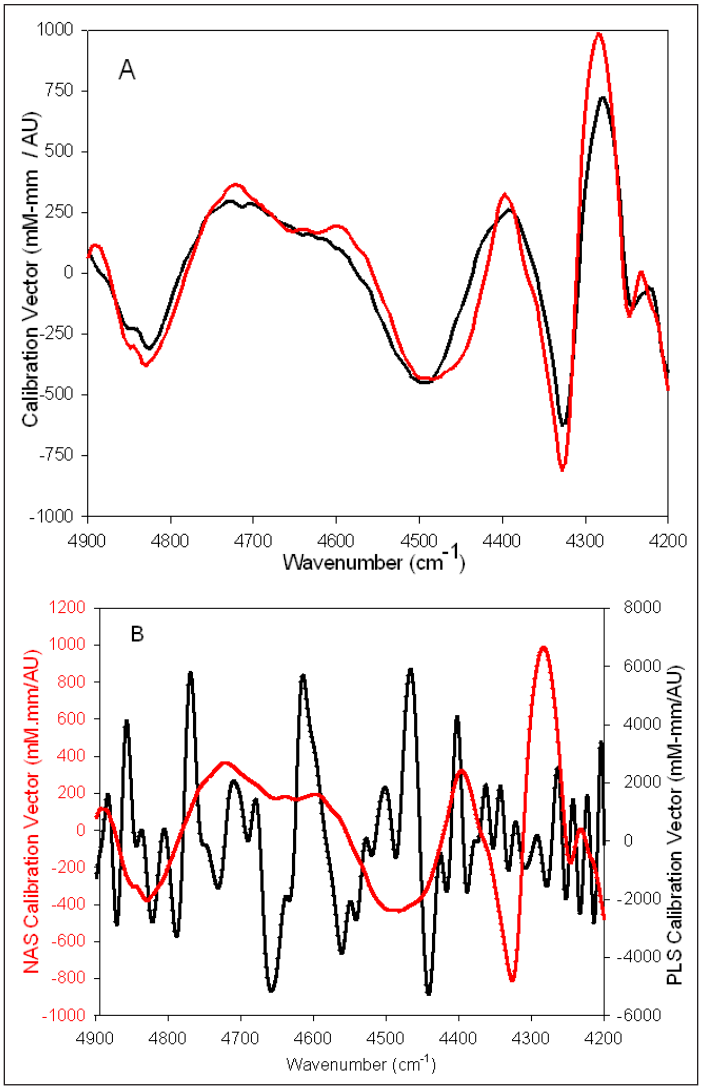

Figure 6. Comparison of PLS (black) and NAS (red) calibration vectors for PLS models generated from noninvasive spectra with correct glucose assignments (**A**) and nonrandom incorrect glucose assignments (**B**).

a collection of baseline noninvasive spectra and the pure component spectrum of glucose dissolved in water. For the NAS vector presented in **Figure 6**, baseline noninvasive spectra were collected during the period of the experiment when the glucose concentration is essentially constant. This constant period extends from 11 to 14 in **Figure 3**. Because glucose levels are constant during this period, variance in baseline noninvasive spectra is assigned to nonglucose-dependent sources and includes variations created by the instrumentation, environment, and sample. This nonglucose-dependent spectral variance is characterized by a set of principal component factors. The NAS vector is obtained as the residual vector after projecting the glucose spectrum vector onto the set of baseline principal component vectors. This process determines the portion of the glucose spectrum that is unique compared to the

nonglucose-dependent spectral variance incorporated in the set of baseline spectra.

A comparison between calibration vectors generated by the PLS algorithm and the NAS calculations reveals a major difference between the PLS calibration vectors created from correct and nonrandom incorrect glucose assignments. **Figure 6A** shows that the PLS calibration vector corresponding to the correct glucose assignments is very similar in shape and magnitude compared to the NAS calibration vector. The similarity between these vectors indicates that the PLS calculation with the correct glucose assignments correctly weighs the glucose selective portion of sample spectra. This finding is significant because the two calibration vectors were generated by using entirely different data analysis procedures. The PLS calibration vector is based on a statistical regression to establish the best correlation between spectral variance and glucose concentration. In contrast, the NAS calibration vector is based on a set of factors that describe the spectral variance and the known absorptivity spectrum of glucose without recourse to a regression step.[9] The convergence of these approaches is significant and lends confidence that both models are in fact based on glucose-specific information present in *in vivo* spectra.

However, **Figure 6B** shows that there is absolutely no similarity between PLS and NAS calibration vectors when incorrect glucose assignments are used in the PLS calculations. The high frequency features below 4400 cm^{-1} in **Figure 6B** strongly suggest that only noise is being modeled in the spectral region most sensitive to glucose, as shown in **Figure 6A**. The poor overlap between these calibration vectors is consistent with a lack of glucose-specific information in the PLS calibration model.

Conclusions

Three critical points can be drawn from these results. First, glucose can be measured selectively from near-infrared spectra collected noninvasively from a rat model. Indeed, the close similarity in the shape and magnitude of the PLS and NAS calibration vectors provides strong evidence that glucose is being measured selectively from these spectra. The knowledge that glucose-specific information is available within *in vivo* near-infrared spectra is critical to the future progress of this field of research.

Second, the apparent functionality of the PLS calibration model based on nonrandom incorrect glucose assignments (**Figure 5**) underscores the propensity to generate false calibration models from this type of analysis. Clearly, results from routine PLS calibration models cannot be accepted at face value and additional corroborating evidence is required to identify the chemical basis of selectivity for the underlying analytical information. The apparent functionality of the false PLS model calls into question the validity of previous reports of successful noninvasive glucose measurements.

Third, analysis of calibration vectors can provide valuable insights into the chemical basis of selectivity for multivariate calibration models. The work described here demonstrates the effectiveness of comparing PLS and NAS calibration vectors. Such an analysis provides powerful corroborating evidence that can supplement a thorough analysis of noninvasive data.[6]

Of course, selectivity is only one requisite requirement for a practical and accurate noninvasive glucose monitor system. Any successful noninvasive glucose monitor must be robust to changes in the environment, instrumentation, and sample. In fact, the results presented here are limited to one set of data collected over a relatively short period of time. Longer term experiments over different forms of glucose transients are needed to test the robustness of such measurements and to determine the frequency of recalibration needed for clinically useful performance. Nevertheless, the ability to distinguish between real (**Figure 6A**) and bogus (**Figure 6B**) calibration models is a major step forward in the advancement of noninvasive glucose methods.

Funding:

This work was supported by grants from the National Institutes of Diabetes and Digestive and Kidney Diseases (DK-60657 and DK-02925).

Acknowledgements:

Portions of the material included in this article were presented during the Diabetes Technology Society Meeting, Technologies for Metabolic Monitoring Session, November 3, 2006.

Disclosures:

J. Olesberg and M. Arnold hold significant equity in the startup company ASL Analytical, Inc. J. Olesberg is a science advisor and M. Arnold is a cofounder and officer of the company.

References:

1. Diabetes Control and Complications Trial Research Group. The effect of intensive treatment of diabetes on the development and progression of long-term complications in insulin-dependent diabetes mellitus. N Engl J Med. 1993 Sep 30;329(14):977-86.

2. Wilson G, Gifford R. Biosensors for real-time *in vivo* measurements. Biosens Bioelectron. 2005 Jun 15;20(12):2388-403.

3. Li CM, Dong H, Cao X, Luong JHT, Zhang X. Implantable electrochemical sensors for biomedical and clinical applications: progress, problems, and future possibilities. Curr Med Chem. 2007;14(8):937-51.

4. Dunn TC, Eastman RC, Tamada JA. Rates of glucose change measured by blood glucose meter and the GlucoWatch Biographer during day, night, and around mealtimes. Diabetes Care. 2004 Sep;27(9):2161-5..

5. Tierney MJ, Kim HL, Burns MD, Tamada JA, Potts RO. Electroanalysis of glucose in transcutaneously extracted samples. Electroanalysis. 2000;12(9):666-71.

6. Arnold MA, Small GW. Noninvasive glucose sensing. Anal Chem. 2005 Sep 1;77(17):5429-39.

7. Khalil OS. Non-invasive glucose measurements at the dawn of the new millennium: an update. Diabetes Technol Ther. 2004 Oct;6(5):660-97.

8. Khalil OS. Spectroscopic and clinical aspects of noninvasive glucose measurements. Clin Chem. 1999 Feb;45(2):165-77.

9. Olesberg JT, Liu L, Van Zee V, Arnold MA. *In vivo* near infrared spectroscopy of rat skin tissue with varying blood glucose levels. Anal Chem. 2006 Jan 1;78(1):215-23.

10. American Society for Testing and Materials. Standard practices for infrared, multivariate, quantitative analysis (E 1655-94). In: Annual book of ASTM standards. Philadelphia (PA): Global Engineering Documents; 1995.

11. Koschinsky T, Heinemann L. Sensors for glucose monitoring: technical and clinical aspects. Diabetes Metab Res Rev. 2001 Mar-Apr;17(2):113-23.

12. Clarke WL, Cox D, Gonder-Frederick LA, Carter W, Pohl SL. Evaluating clinical accuracy of systems from self-monitoring of blood-glucose. Diabetes Care. 1987 Sep-Oct;10(5):622-8.

13. Lorber A. Error propagation and figures of merit for quantification by solving matrix equations. Anal Chem. 1986;58:1167-72.

14. Lorber A, Faber K, Kowalski BR. Net analyte signal calculation in multivariate calibration. Anal Chem. 1997;69(8):1620-6.